UMYU Scientifica, Vol. 5 NO. 2, June 2026, Pp 323 – 335
https://doi.org/10.56919/usci.2652.030
ISSN: 2955 – 1145 (print); 2955 – 1153 (online)
A periodical of the Faculty of Natural and Applied Sciences, UMYU, Katsina

ORIGINAL RESEARCH ARTICLE

A Preliminary Evaluation of a Depth-Weighted Geoelectrical Vulnerability Index for Basement Aquifer at Federal University of Health Sciences, Ila-Orangun

Warith Adewale Adebisi[1, 2]*, Saminu Olatunji[2] and Hussain Olanrewaju Abubakar[2]
1Department of Physical and Chemical Sciences, Federal University of Health Sciences, Ila-Orangun, Osun State, Nigeria
2Department of Geophysics, University of Ilorin, Ilorin, Nigeria

ABSTRACT
Assessing intrinsic groundwater vulnerability in crystalline basement terrains remains challenging because conventional vulnerability approaches often fail to account for the vertical distribution of the protective subsurface layer. This study presents a depth-weighted geoelectric vulnerability index (DWGVI) designed to incorporate the depth-dependent effectiveness of protective layers in basement aquifer systems. Electrical resistivity data from thirty vertical electrical sounding (VES) points were quantitatively interpreted to derive layer resistivity and thickness parameters. The DWGVI was formulated using the depth-weighted Dar Zarrouk principle, while longitudinal conductance (S) was computed as a conventional indicator of aquifer protective capacity for comparison. Results reveal a multilayered basement aquifer system characterized by thin overburden and shallow fractured bedrock. Longitudinal conductance values ranged from 0.0155 to 0.1439 S, indicating predominantly weak to moderate protective capacity, whereas DWGVI values varied between 0.00744 and 0.06829 S/m. Following normalization, the derived vulnerability index delineated zones of very low, low, moderate, high and very high intrinsic vulnerability across the study area. Pearson correlation analysis revealed a statistically significant moderate positive relationship between DWGVI and longitudinal conductance ($r = 0.607$ $\rho = 0.00038$), while Spearman's rank correlation indicated a stronger monotonic association ($\rho = 0.740$, $\rho = 0.001$), suggesting that both indices respond similarly to variations in subsurface resistivity and thickness. However, because the proposed index has not been independently validated using hydrochemical or borehole datasets, its wider applicability requires further investigation in other crystalline basements. The findings demonstrate that incorporating depth-weighting significantly can improve the hydrogeological realism of geoelectrical vulnerability assessment in basement terrains.

ARTICLE HISTORY
Received March 19, 2026
Accepted June 26, 2026
Published June 29, 2026

KEYWORDS
Vulnerability index, Longitudinal Conductance, DWGVI, Dar Zarrouk, Overburden.

INTRODUCTION
Groundwater resources play a critical role in meeting domestic, agricultural and institutional water demands, particularly in areas where surface water availability is limited or unreliable (Alao et al., 2024; Karandish et al., 2025; Li & Elumalai, 2025). In many parts of sub-Saharan Africa, including southwestern Nigeria, basement aquifers constitute the primary source of portable water (Idowu & Ojo, 2024; Nyika & Dinka, 2023; Ohenhen et al., 2023). These aquifers are inherently vulnerable to contamination due to their unique hydrogeological characteristics, which distinguish them fundamentally from sedimentary aquifer systems. Basement aquifers are typically characterized by shallow water tables, thin and discontinuous overburden, and groundwater occurrence largely controlled by secondary porosity in weathered and fractured zones (Akanbi, 2018). Unlike sedimentary aquifers, where thick, laterally extensive clay layers may provide significant natural protection, crystalline basement aquifers often lack continuous confining units (Egbueri et al., 2025). As a result, contaminants introduced at the surface can rapidly migrate into the subsurface through permeable regolith or interconnected fracture networks, posing a substantial risk to groundwater quality (Barranco et al., 2012). The presence of fracture-controlled flow paths further exacerbates this vulnerability by facilitating preferential, and often rapid, contaminant transport that bypasses the limited natural filtration capacity of the overburden.

Assessing groundwater vulnerability in basement terrains, therefore, requires an approach that adequately captures the combined effects of overburden properties, aquifer depth, and structural controls (Akinwumiju & Olorunfemi, 2018; Sharp, 2014). Traditional groundwater vulnerability assessment methods, such as DRASTIC,

Correspondence: Warith Adewale Adebisi. Department of Physical and Chemical Sciences, Federal University of Health Sciences, Ila-Orangun, Osun State, Nigeria. ✉ warith.adebisi@fuhsi.edu.ng **and 16-68en001.pg@students.unilorin.edu.ng**
How to cite: Adebisi, W. A., Olatunji, S., & Abubakar, H. O. (2026). A Preliminary Evaluation of a Depth-Weighted Geoelectrical Vulnerability Index for Basement Aquifer at Federal University of Health Sciences, Ila-Orangun. *UMYU Scientifica*, 5(2), 323 – 335. https://doi.org/10.56919/usci.2652.030

GOD, and related index-based models, were originally developed for sedimentary environments where aquifer systems are relatively homogeneous and stratified (Barbulescu, 2020; Fannakh & Farsang, 2022; Maria, 2018). These methods often rely on parameters such as soil type, depth to water, and recharge rate, which may not be readily available or appropriately representative in crystalline terrains (Patel et al., 2022). Consequently, the direct transfer of such indices to basement aquifers can lead to misleading vulnerability estimates and inadequate groundwater protection strategies.

Aquifer protective capacity refers to the ability of overlying geological materials to attenuate or retard the downward migration of contaminants before they reach the groundwater system (Alao et al., 2023; Ikpe et al., 2025). Intrinsic groundwater vulnerability describes the inherent susceptibility of an aquifer to contamination based on its natural hydrological characteristics, independent of the nature and magnitude of contaminant loading (Barbulescu, 2020). Contamination risk, however, represents the combined effect of intrinsic vulnerability and the presence, intensity and probability of contamination sources.

Geophysical approaches, particularly electrical resistivity methods, have been widely used as cost-effective tools for evaluating the protective capacity of aquifers in data-scarce basement regions (Adamu et al., 2025; Lawal & Usman, 2022; Sani et al., 2025; Shuaibu, 2024; Hassan & Rilwanu, 2025). Parameters derived from vertical electrical sounding (VES), such as overburden thickness and longitudinal conductance, have been extensively used as proxies for intrinsic aquifer protection (De Almeida et al., 2021). While these parameters provide valuable insights, they implicitly assume that all protective layers contribute equally to aquifer protection, regardless of their depth below the surface (Jain, 2023). This assumption is problematic in basement terrains, where the effectiveness of the protective layer is strongly influenced by its position relative to the surface and the aquifer. Shallow, low-resistivity layers can significantly attenuate contaminant migration, whereas deeper, conductive layers may offer limited protection despite contributing high conductance (You et al., 2020).

This limitation highlights a critical gap in existing geoelectrical vulnerability indices: the inadequate representation of depth-dependent protection in crystalline basement aquifers. Current indices largely neglect the vertical distribution of protective materials, thereby oversimplifying the complex interactions among lithology, thickness, and depth. As a result, areas with deep but conductive layers may be incorrectly classified as well-protected, even when the aquifer is effectively exposed to surface-derived contamination. In response to this challenge, there is a growing need for vulnerability assessment that explicitly incorporates the depth dependence of protective layers in the basement aquifer system. Integrating depth-weighted geoelectrical parameters provides a more realistic representation of intrinsic vulnerability by accounting for the decrease in the protective efficiency of overburden materials with depth. Such an approach is particularly suited to crystalline terrains, where shallow weathered layers and fracture networks dominate groundwater recharge and flow dynamics. This study addresses this gap by proposing a depth-weighted geoelectrical index designed to improve the evaluation of groundwater vulnerability in basement aquifers.

The inverse-depth weighting scheme adopted in this study is founded on the premise that the effectiveness of a protective layer decreases with increasing distance from the ground surface. Contaminants introduced at the land surface interact rapidly with shallow subsurface materials, thereby exerting the greatest influence on attenuation processes such as adsorption, filtration, and dispersion (Omo-Okoro et al., 2025). Conversely, deeper conductive layers, although potentially contributing substantially to cumulative conductance, may provide limited practical protection if overlying strata permit rapid contaminant transmission (Udosen et al., 2024). By assigning greater weight to shallow protective layers, the proposed inverse-depth seeks to better represent the hydrogeological significance of near-surface materials in basement aquifer environments with thin overburden. This study hypothesizes that incorporating the vertical position of protective layers into geoelectrical vulnerability assessment will yield a different representation of intrinsic vulnerability compared with conventional longitudinal-conductance methods that do not explicitly account for depth-dependent protective effectiveness.

This study aims to develop and apply a depth-weighted geoelectrical index to evaluate the intrinsic groundwater vulnerability of basement aquifers, with a view to improving vulnerability assessment in crystalline basement terrains, where conventional indices are often inadequate. To achieve this aim, the study seeks to derive subsurface layer resistivity and thickness parameters through quantitative interpretation, formulate a depth-weighted geoelectrical vulnerability index that explicitly incorporates the vertical position of protective layers relative to aquifer depth, compare the performance of the proposed depth-weighted index with the conventional longitudinal conductance method commonly used for aquifer protective capacity assessment and produce a groundwater vulnerability zoning maps based on the proposed index to delineate areas of varying intrinsic vulnerability. This study presents an analytical extension of earlier geophysical investigations in the area (Adebisi et al., 2026), with the emphasis shifted from aquifer characterization to vulnerability assessment using a newly developed depth-weighted index.

Although the geoelectrical dataset utilized in this study was previously interpreted for groundwater potential evaluation by Adebisi et al. (2026), the objective and analytical framework of the present investigation are fundamentally different. The earlier study focused on identifying favourable groundwater accumulation zones using integrated magnetic and electrical methods. In contrast, this study re-analyses the interpreted VES models to develop and evaluate a depth-weighted geoelectrical vulnerability index to assess the intrinsic

susceptibility of the aquifer system to surface-derived contamination. Thus, the novelty of the work lies not in acquiring new geophysical data but in formulating and applying a depth-sensitive vulnerability that explicitly accounts for the vertical distribution of protective layers.

STUDY AREA DESCRIPTION

The study area is within the premises of the Federal University of Health Sciences, Ila-Orangun (Adebisi et al., 2026). The area is located within the crystalline Basement complex of southwestern Nigeria and is characterized by increasing reliance on groundwater for domestic and institutional water supply. Climatically, the area experiences a tropical humid regime with distinct wet and dry seasons. Annual rainfall is moderate to high, promoting active groundwater recharge through infiltration (Abd-Elaty et al., 2024), particularly during the rainy season. While this enhances groundwater availability, it also facilitates the downward migration of surface-derived contaminants. The geological and hydrogeological descriptions are adapted from earlier investigations of the area (Adebisi et al., 2026). Geologically, the area is underlain by Precambrian crystalline rocks comprising predominantly granites, gneisses, and schists (Obaje, 2009). Groundwater occurrence is restricted to the weathered regolith and fractured basement zones, where secondary porosity and permeability control storage and flow. The overburden consists of topsoil, clayey to sandy weathered materials and partially fractured bedrock. Hydrogeologically, the aquifer system is confined to semi-confined, with shallow water tables in many parts of the area (Adebisi et al., 2026). Institutional facilities and agricultural activities dominate land-use patterns in the study area. Waste disposal practices, including the use of septic tanks and refuse dumps, are poorly regulated and sited without adequate consideration of the subsurface.

MATERIALS AND METHODS

The geophysical dataset utilized in this study was originally acquired and interpreted in a previous investigation by Adebisi et al. (2026) and is re-analyzed here using a new vulnerability modelling framework. Permission to conduct the geophysical survey was obtained from the relevant university authorities during the original data acquisition stage. The study involved non-invasive geophysical measurement and did not include human or animal subjects. The survey employed an ABEM Terrameter SAS 1000 resistivity meter. Electrical resistivity data for this study were acquired using the vertical electrical sounding (VES) technique, which is well-suited for investigating the vertical variation of subsurface electrical properties in basement complex terrains. The Schlumberger electrode configuration was adopted due to its sensitivity to changes in layer resistivity and thickness, as well as its widespread application in groundwater vulnerability studies (Oyeyemi et al., 2022). A total of thirty VES points were established across the study area to ensure adequate spatial coverage and to capture lateral variations in subsurface conditions relevant to aquifer vulnerability. The sounding locations were strategically selected based on accessibility, land-use distribution and geological variability, with emphasis on areas of high groundwater abstraction and potential contamination sources. Details of the apparent resistivity measurements, electrode spacing and complete VES metadata for VES 1 to VES 10 is provided in the Table 1 below.

At each VES station, the current electrode separation (AB) was progressively increased symmetrically about the centre point while maintaining relatively small potential electrode spacing (MN). The maximum half-current electrode spacing (AB/2) employed in the survey was 100 m, which provided sufficient depth of investigation to resolve the overburden sequence and the top of the basement aquifer. Apparent resistivity values were computed from the measured field resistances using the appropriate geometric factor for the Schlumberger array. The acquired apparent resistivity data were subjected to quantitative interpretation through a combination of partial curve matching and computer-assisted inversion. Initial model parameters were obtained from standard master curves, and iterative inversion using Winresist software was performed to obtain the true layer resistivities and thicknesses. The quality of the inversion was assessed using the root-mean-square (RMS) error reported by the software. The resulting geoelectrical models formed the basis for deriving subsurface parameters used in the subsequent vulnerability assessment.

Longitudinal Conductance

The longitudinal conductance (S) method was employed in this study as a conventional geoelectrical indicator of aquifer protective capacity for comparative evaluation with the proposed depth-weighted geoelectrical vulnerability index (Adebisi et al., 2026; Bayewu et al., 2018; Tijani et al., 2021). The longitudinal conductance at each VES location was calculated using the standard formulation:

$$S = \sum_{i=1}^{n} \frac{h_i}{\rho_i} \quad (1)$$

S is the longitudinal conductance measured in Siemens, ρ_i is the true resistivity ($\Omega.m$) of the ith subsurface layer, h_i is the thickness (m), and n is the number of geoelectrical layers overlying the aquifer.

Depth-Weighted Geoelectrical Vulnerability Index (DWGVI)

The depth-weighted geoelectrical vulnerability index (DWGVI) is formulated to quantify the intrinsic vulnerability of basement aquifers by explicitly incorporating the depth-dependent effectiveness of protective subsurface layers. Aquifer units were identified based on the integrated interpretation of layer resistivity characteristics, thickness and established hydrogeological understanding of the basement terrains. Weathered layers exhibiting moderate resistivity values and fractured basement horizons with resistivity lower than that of fresh basement were interpreted as potential aquifer units. Only geoelectrical layers overlying the identified aquifer horizon

were included in the DWGVI computations, as these constitute the protective materials influencing contaminant attenuation prior to reaching the groundwater system.

Table 1: VES Field Parameters and Corresponding Apparent Resistivity for VES 1 - 10

			Rho (Ohm.m)									
AB/2 (m)	**MN/2 (m)**	**G (m)**	**VES 1**	**VES 2**	**VES 3**	**VES 4**	**VES 5**	**VES 6**	**VES 7**	**VES 8**	**VES 9**	**VES 10**
1	0.25	5.89	363.29	250.62	294.35	362.12	269.19	169.66	352.63	310.14	285.98	954.05
1.3	0.25	10.23	288.28	273.75	294.52	365.31	223.73	158.16	294.52	334.52	265.37	939.32
1.8	0.25	19.97	233.68	258.05	272.23	320.96	209.32	140.83	243.87	232.88	186.35	763.96
2.4	0.25	35.81	216.81	258.35	272.93	269.64	164.31	134.8	212.8	180.35	142.46	600.94
3.2	0.25	63.97	178.29	253.2	290.31	251.22	130.18	110.61	197.16	167.93	104.15	452.99
4.2	0.25	110.49	157.33	242.74	298.98	216.89	119.11	100.28	177.55	187.72	86.56	224.84
4.2	1	26.15	171.33	287.11	265.93	195.7	187.04	107.73	136.21	174.25	104.8	265.93
5.5	1	45.96	184.22	269.81	282.45	170.67	166.02	97.72	164.6	198.75	93.03	147.78
7.5	1	86.82	193.44	266.72	281.74	152.81	131.62	91.86	161.66	218.18	113.04	118.34
10	1	155.57	193.06	283.3	276.92	135.49	139.92	111.11	169.26	242.07	143.72	142.88
13	1	264	210.04	311.52	266.64	102.59	87.57	142.08	195.54	279.31	182.93	132.42
13	2.5	102.3	223.73	274.78	297.69	138.41	90.45	153.96	183.12	237.13	176.88	96.8
18	2.5	199.73	353.52	270.23	295.2	181.75	115.08	207.12	264.04	268.24	226.89	89
24	2.5	358.13	324.64	279.13	281.49	253.05	103.11	291.87	345.81	357.09	264.73	122.05
32	2.5	639.73	440.01	306.56	328.69	332.66	129.48	414.61	472.57	401.94	326.84	185.01
42	2.5	1104.87	566.58	387.81	429.35	428.58	153.91	550.78	622.71	606.8	478.85	259.42
55	2.5	1897.5	735.47	517.26	608.15	596.57	184.76	669.82	799.23	833.95	541.93	385.38
55	5	942.86	727.32	510.37	595.51	600.22	225.34	761.64	823.11	926.92	611.07	499.53
75	5	1760	900.94	841.63	472.56	422.4	122.11	830.9	1065.5	1033.12	821.92	696.61
100	5	3135	1256.82	1349.3	523.23	415.7	144.49	884.7	1476.9	1464.05	1199.14	872.16

The index is derived from geoelectrical parameters obtained through VES interpretation and considers only the layers overlying the aquifer unit. For a given VES location, the DWGVI is defined as:

$$\mathrm{DWGVI} = \sum_{i=1}^{n} \left(\frac{h_i}{\rho_i} \times \frac{1}{z_i} \right) \quad (2)$$

Where h_i = thickness of the ith subsurface layer (m), ρ_i = true resistivity of the ith layer (Ωm), z_i = depth to the

midpoint of the ith layer measured from the ground surface (m), and n = total number of geoelectrical layers above the aquifer.

The term $\frac{h_i}{\rho_i}$ denotes the protective contribution of each layer, analogous to the classical concept of longitudinal conductance, in which thicker, more conductive layers provide greater resistance to contamination migration. However, unlike conventional indices, the DWGVI introduces an explicit depth-weighting factor, $\frac{1}{z_i}$, to account for the diminishing protective effectiveness of deeper layers. By applying inverse depth weighting, layers closer to the surface exert a stronger influence on the index, reflecting their greater capacity to intercept infiltrating contaminants at early stages. Conversely, deeper layers contribute progressively less to overall protection, even when they possess favourable resistivity and thickness characteristics. This formulation aligns with contaminant transport dynamics in basement terrains, where shallow permeable zones and fracture networks often dominate vertical flow. High DWGVI values indicate strong protective capacity and low intrinsic vulnerability, typically associated with shallow, thick, low-resistivity layers. Low DWGVI values indicate weak protection and high intrinsic vulnerability, commonly occurring where overburden is thin, resistive, or located at greater depths.

To enable spatial comparison and facilitate vulnerability mapping, the computed DWGVI values were normalized using min-max scaling. Normalization transforms raw DWGVI values into a dimensionless index with a uniform range. The normalized DWGVI was computed as:

$$\mathrm{DWGVI_n} = \frac{\mathrm{DWGVI} - \mathrm{DWGVI_{min}}}{\mathrm{DWGVI_{max}} - \mathrm{DWGVI_{min}}} \quad (3)$$

Where DWGVI represents the computed index at a given VES location, while $\mathrm{DWGVI_{min}}$ and $\mathrm{DWGVI_{max}}$ denote the minimum and maximum values obtained across the study area, respectively. This transformation constrains the normalized index to values between 0 and 1, enabling consistent comparisons across locations. Following normalization, the $\mathrm{DWGVI_n}$ values were classified into five intrinsic groundwater vulnerability classes based on their relative magnitudes using the natural break (Jenks) algorithm, which identifies inherent groupings within the data.

Statistical Analysis

Statistical analyses were carried out to evaluate the relationship between the DWGVI and the conventional longitudinal conductance (S) and to assess the robustness of the index. The analysis was performed using standard descriptive and inferential statistical techniques. The computed DWGVI and S values obtained at corresponding VES locations were compiled into a unified dataset to ensure one-to-one comparison. Descriptive statistics, including minimum, maximum, mean and standard deviation, were used to summarise the distribution and variability of both indices across the study area. To quantify the degree of association between DWGVI and S, correlation analysis was conducted. Pearson's correlation coefficient (r) was employed to assess the strength and direction of the linear relationship between the two indices. In addition, Spearman's rank correlation coefficient (p) was computed as a non-parametric measure to evaluate the monotonic relationship between DWGVI and S. Statistical significance of the correlation was evaluated using corresponding p-values, with significance assessed at the 95% confidence level ($p<0.05$). Scatter plots were generated to visually examine the trends and discrepancies between the indices.

RESULTS AND DISCUSSIONS

Interpretation of the VES data reveals a multilayered subsurface typical of crystalline basement terrain. The summary of the geo-electric parameters of the VES is presented in Table 2.

Interpretation of the 30 VES data reveals a multilayered subsurface typical of crystalline basement terrains. Representative 1D inversion curves of sampled VES stations showing calculated apparent resistivity and computed model are displayed in Figure1 and Figure 2. The geoelectrical succession generally comprises a thin topsoil, an underlying sandy clay-to-clayey sand unit, a weathered basement layer, and a fractured to fresh basement bedrock. The topsoil exhibits highly variable resistivity values ranging from approximately 102 to 10862 $\Omega.\mathrm{m}$, with thickness varying between 0.5 and 4.7 m. The large resistivity variation reflects the presence of lateritic hardpan in some locations.

The second layer, interpreted as sandy clay or clayey sand, shows resistivity values between 73 and 691 $\Omega.\mathrm{m}$ and a thickness of 1.1 to 4.9 m. This unit constitutes the primary near-surface protective layer in the study area. The weathered layer displays resistivity values ranging from 54 to 1664 $\Omega.\mathrm{m}$ and a thickness between 2.2 and 15.1 m. In several locations, this unit serves as the main aquifer, provided it is sufficiently fractured and saturated. The fractured basement, identified as the principal groundwater bearing unit, occurs at depths ranging from approximately 3.6 m to 24.5 m, indicating generally shallow aquifer conditions across the study area. Curve type analysis reveals that HA-type curves dominate (40%), followed by QH-type (20%). The predominance of HA and QH curves suggests the widespread occurrence of conductive intermediate layers underlain by some more resistive basement, consistent with typical basement complex hydrogeology.

Table 3 summarises the aquifer longitudinal conductance and the computed depth-weighted geoelectrical vulnerability index across the VES points. Computation of S and DWGVI is shown in the Appendix. Higher DWGVI values indicate stronger protective effectiveness of overlying strata, whereas lower DWGVI values correspond to reduced attenuation potential and, consequently, greater intrinsic groundwater vulnerability.

Table 2: Summary of geoelectrical resistivity and thickness ranges

VES Point	Curve Type	Resistivity (Ωhm. m) $\rho_1/\rho_2/\rho_3/\ldots/\rho_n$	Thickness (m) $h_1/h_2/h_3/\ldots/h_n/-$	Inferred Lithology
1	QH	342/148.9/97.5/173.8	0.5/3.3/11.3/-	Topsoil/Sandy clay/Weathered basement/Weathered basement
2	AH	311.7/341.9/70/759.1	0.8/1.3/4.6/-	Topsoil/Sandy clay/weathered basement/Fractured basement
3	HAK	296.3/270/279/351/2147	0.7/1.1/12.7/22.7/-	Topsoil/Clayey sand/Sandy clay/Fractured basement/Fresh basement
4	KQH	252.8/284.6/250.6/194.1/11545.5	1.1/2.2/8.3/9.2/-	Topsoil/laterite/sandy clay/weathered basement/fresh basement
5	HA	433.7/137.3/214.5/7671.7	0.7/1.9/11.5/-	Topsoil/Clay/Weathered basement/fresh basement
6	QHK	175.9/94.9/56.1/10429/1834	1.1/1.1/3.5/24.5/-	Topsoil/Sandy clay/Weathered basement/Fresh basement/Basement
7	QH	357.8/169.2/129/14984	0.7/1.1/7.6	Topsoil/Sandy clay/Weathered basement/Fractured basement
8	HA	457.8/142.5/257/9962.5	0.6/2.1/12.8/-	Topsoil/Sandy clay/Weathered basement/Fractured basement
9	HA	359.5/72.9/929.1/6709.8	0.8/4.8/13.9/-	Topsoil/Weathered material/Weathered basement/Fresh basement
10	QH	10861.7/129.6/72.5/17231.4	1.2/2.9/8.8/-	Lateritic topsoil/Clayey sand/Weathered basement/Fresh basement
11	QH	2827/117.9/53.7/29309	0.5/1.8/3.6/-	Lateritic topsoil/Clayey sand/Weathered basement/Fresh basement
12	QH	2206.3/660.3/71.4/13417.4	0.9/3.1/6.3/-	Lateritic topsoil/Dry sandy layer/ Weathered basement/Fresh basement
13	KH	101.7/420.2/217.8/2612.6	4.7/2/7/-	Topsoil/Sandy clay/Weathered basement/Fractured basement
14	HAA	568/124.3/362/1056.7/4756.4	0.5/2.3/8.5/15.6/-	Topsoil/Sandy clay/Weathered basement/Fractured basement /Fresh basement
15	HAA	264.9/140.4/260.3/370.9/15129	0.6/3.1/3/1.7/-	Topsoil/Sandy clay/Weathered basement/Weathered basement/Fresh basement
16	HA	185.1/112.4/615.9/24681.2	0.9/2.1/9.5/-	Topsoil/Sandy clay/Weathered basement/Fresh basement
17	HA	104.6/84.2/481.3/5023.9	0.6/4.2/5.8/-	Topsoil/Sandy clay/Weathered basement/Fractured basement
18	HKH	274.3/89.4/270.5/74.1/3493.6	0.5/1.2/2.2/5.3/-	Topsoil/Sandy clay/Weathered basement/Weathered basement/Fresh basement
19	QHA	550.4/542.8/219.2/3468.5/25426.3	0.8/2.1/5.8/11.5/-	Topsoil/Sandy clay/Weathered basement/Fractured basement/Fresh basement
20	QH	352.2/278.7/140.2/18419.6	0.7/3.5/6.7/-	Topsoil/Sandy clay/Weathered basement/Fractured basement
21	HKH	353.2/235/606.7/165.9/27448.7	0.5/2/2.7/5.4/-	Topsoil/Sandy clay/Dry sand/Fractured basement/Fresh basement
22	HA	359.3/105.5/616.5/30234.4	0.6/1.5/15.1/-	Topsoil/Sandy clay/Weathered basement/Fractured basement

To be continued next page

Table 2 continued

VES Point	Curve Type	Resistivity (Ωm) $\rho_1/\rho_2/\rho_3/\ldots/\rho_n$	Thickness (m) $h_1/h_2/h_3/\ldots/h_n/-$	Inferred Lithology
23	HA	317.6/271.8/1553.5/4883.7	0.7/4.6/15/-	Topsoil/Weathered basement/Fractured basement/Fresh basement
24	HA	351.6/170.4/407.5/7590.5	0.9/2.1/12.4/-	Topsoil/Sandy clay/Weathered basement/Fractured basement
25	HA	520.9/462/675/27621.9	0.8/3.8/6.1/-	Topsoil/Sandy clay/Weathered basement/Fractured basement
26	AA	629.4/690.5/1459.5/4012.9	0.7/4.9/10.6/-	Topsoil/Lateritic clay/Fractured basement/Fresh basement
27	HA	558.7/314/1045/2075.5	0.8/1.4/13.6/-	Topsoil/Lateritic clay/Fractured basement/Fresh basement
28	AAA	313.4/478/1663.9/1986/12886.9	1.2/2.9/12/16.3/-	Topsoil/Lateritic clay/Fractured basement/Fractured basement/Fresh basement
29	HA	355.3/310.4/626.4/4701.3	0.9/1.9/8.1/-	Topsoil/Sandy clay/Weathered basement/Fresh basement
30	HA	289.9/112.2/571.2/23311.5	0.5/1.4/14.2/	Topsoil/Sandy clay/Weathered basement/Fresh basement

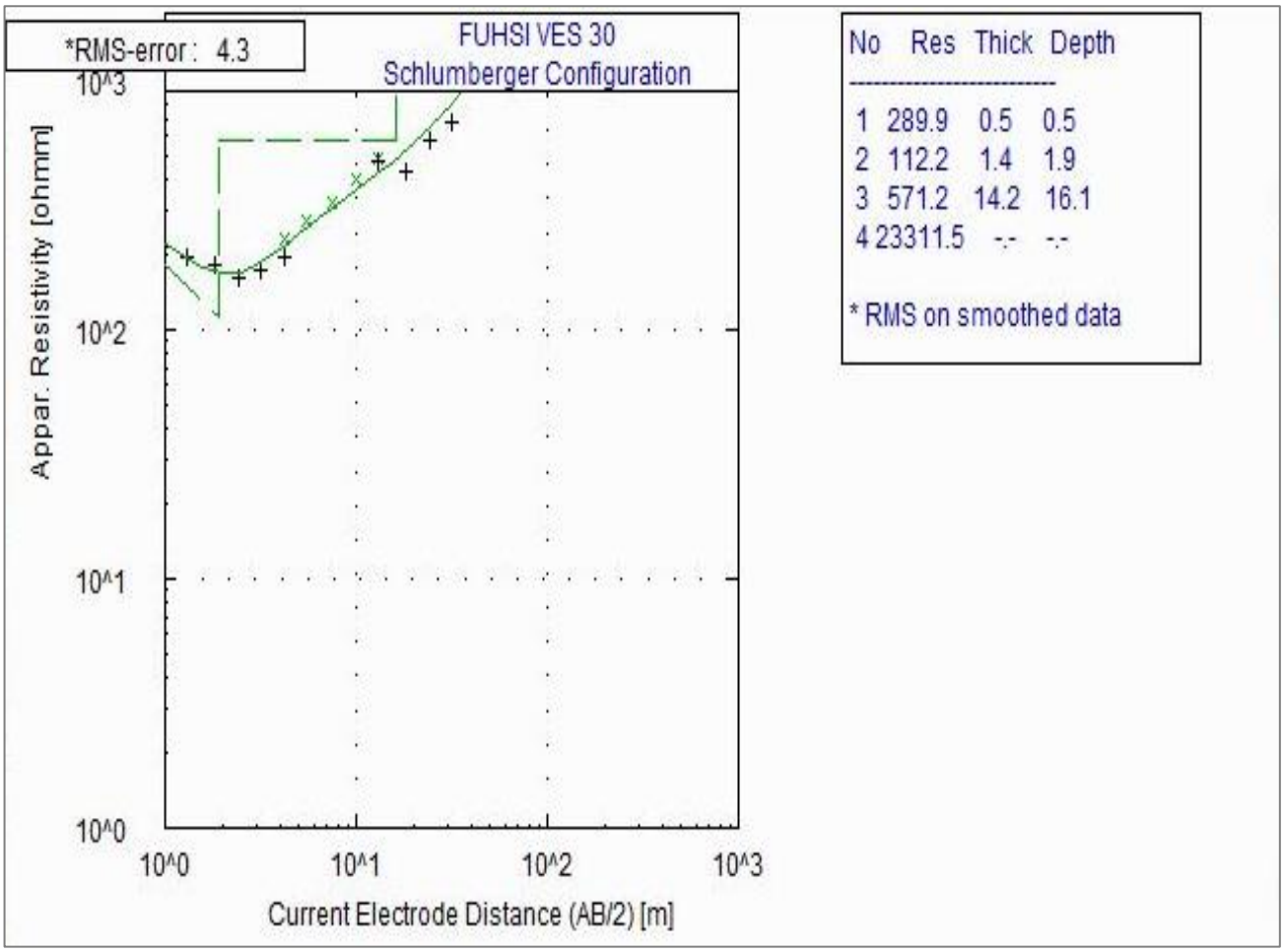

Figure 1: Sample four-layer curve type obtained at VES 30

Computed Longitudinal Conductance and DWGVI and Normalized DWGVI Values

The computed longitudinal conductance values across the 30 VES locations range from 0.0155 S to 0.1439 S, with a mean of 0.0630±0.0341 S, indicating predominantly weak to moderate aquifer protective capacity. The DWGVI ranges from 0.00744 S/m to 0.06829 S/m, with a mean of 0.0309±0.0146 S/m, reflecting substantial spatial heterogeneity in the thickness, resistivity, and vertical positioning of the protective layers.

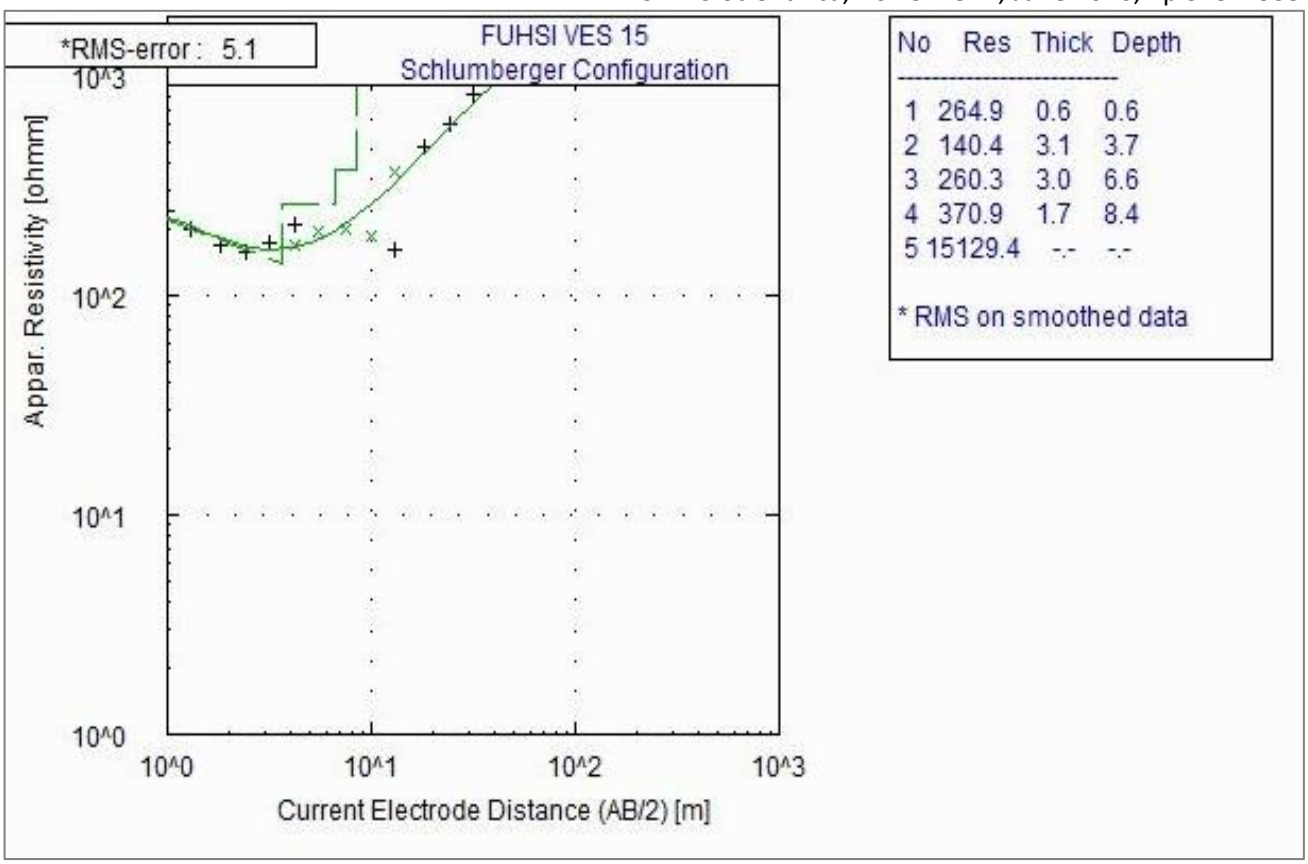

Figure 2: Sample five-layer curve type obtained at VES 15

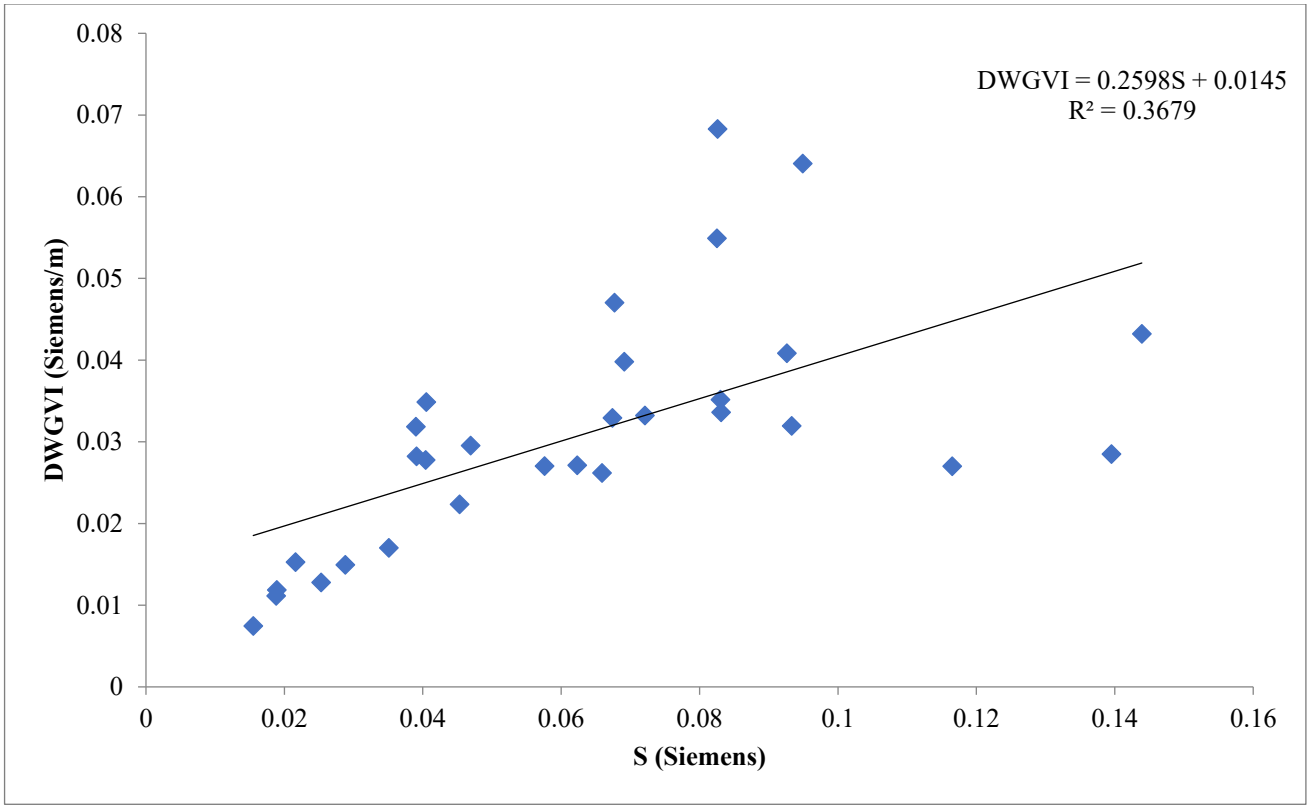

Figure 3: Relationship between DWGVI and S

Table 4 shows the correlation statistics between S and DWGVI. Pearson correlation analysis yielded a coefficient of $r = 0.607$ ($p = 0.00038$), indicating a statistically significant moderate positive linear relationship between the two indices. Linear regression analysis yielded the equation DWGVI = 0.2598S + 0.0145, indicating that DWGVI increases with increasing S values (Figure 3). Spearman's rank correlation further showed a stronger monotonic association ($\rho = 0.740$, $p = 0.001$), suggesting that both indices respond similarly to variations in subsurface resistivity and thickness.

Table 3: Summary of longitudinal conductance and computed DWGVI

Longitude	Latitude	VES NO	S (S)	DWGVI (S/m)	Normalized DWGVI	Vulnerability
4.947578	8.015122	1	0.0691	0.039793	0.531667	Moderate
4.947610	8.015575	2	0.0926	0.040838	0.548841	Moderate
4.947690	8.016020	3	0.1165	0.027009	0.321562	High
4.947737	8.016438	4	0.0721	0.033224	0.423700	Moderate
4.947787	8.016858	5	0.1395	0.028502	0.346099	High
4.947552	8.014717	6	0.0826	0.068287	0.999998	Very Low
4.947462	8.014248	7	0.0674	0.032914	0.418610	Moderate
4.947442	8.013790	8	0.0659	0.026186	0.308030	High
4.947397	8.013335	9	0.0830	0.035151	0.455374	Moderate
4.947152	8.012780	10	0.1439	0.043202	0.587710	Moderate
4.947067	8.012427	11	0.0825	0.054915	0.780213	Low
4.946950	8.011995	12	0.0933	0.031947	0.402712	Moderate
4.946878	8.011552	13	0.0831	0.033608	0.430019	Moderate
4.946762	8.011118	14	0.0576	0.027029	0.321884	High
4.946662	8.010657	15	0.0405	0.034871	0.450772	Moderate
4.946542	8.010227	16	0.0390	0.031846	0.401056	Moderate
4.946428	8.009827	17	0.0677	0.047029	0.650600	Low
4.946160	8.008730	18	0.0949	0.064047	0.930304	Very Low
4.945442	8.019887	19	0.0351	0.017019	0.157366	Very High
4.945577	8.019460	20	0.0623	0.027120	0.323385	High
4.945760	8.019035	21	0.0469	0.029541	0.363177	High
4.945842	8.018597	22	0.0404	0.027768	0.334031	High
4.945952	8.018182	23	0.0288	0.014943	0.123245	Very High
4.946115	8.017763	24	0.0453	0.022333	0.244711	High
4.946387	8.017417	25	0.0188	0.011131	0.060600	Very High
4.946637	8.017055	26	0.0155	0.007444	0	Very High
4.946855	8.016658	27	0.0189	0.011863	0.072623	Very High
4.946678	8.016268	28	0.0253	0.012775	0.087608	Very High
4.946440	8.015885	29	0.0216	0.015265	0.128540	Very High
4.946158	8.015525	30	0.0391	0.028226	0.341555	High

Table 4: Correlation statistics between S and DWGVI

Statistic	Value
Pearson's (r)	0.607
p-value	0.00038
Spearman's (ρ)	0.740
p-value	0.001
Sample size	30

However, the correlation is not perfect, reflecting the influence of depth-weighting in the DWGVI formulation. This divergence indicates that while both indices capture general protective trends, the DWGVI introduces additional sensitivity to the vertical distribution of protective layers, thereby providing enhanced hydrogeological realism for vulnerability assessment in basement aquifer systems.

Following min-max normalization, $DWGVI_n$ values range from 0 to approximately 1.0. High normalised values (>0.75) observed at VES 6, VES 18, and VES 11 correspond to locations where relatively thick, moderately conductive weathered materials occur close to the surface, thereby increasing effective aquifer protection under the depth-weighted framework. In contrast, very low normalized values at VES 26, VES 25, and VES 27 indicate zones of high intrinsic vulnerability, characterized by thin overburden and a shallow fractured basement. Although some locations exhibit high longitudinal conductance, such as VES 5 and 10, their $DWGVI_n$ values are only moderate, demonstrating that depth-independent conductance may overestimate protection where conductive layers occur at greater depth. Conversely, VES 6 shows only a moderate S value but the highest DWGVI, highlighting the strong influence of shallow protective layers in the depth-weighted approach. Overall, the results confirm that intrinsic groundwater vulnerability in the study area is primarily controlled by shallow aquifer occurrence and the vertical distribution of clay-rich weathered materials, and they demonstrate that incorporating depth-dependent weighting provides a more realistic representation of protective effectiveness in the basement aquifer system than conventional longitudinal conductance alone.

Figure 4 shows the spatial distribution maps of the longitudinal conductance and the depth-weighted geoelectrical vulnerability index. The longitudinal conductance map displays relatively smooth gradients, with moderate protective zones extending across much of the central and southern parts, reflecting its cumulative

integration of layer thickness and conductivity without accounting for depth. Areas with deeper conductive layers, particularly around VES 10–12 and in the southern part, show relatively elevated conductance values that may overstate aquifer protection. In contrast, the DWGVI map presents sharper spatial contrasts and a more hydrogeologically consistent vulnerability structure. High-protection zones in the north-central portion around VES 24 – 28 show that they are more distinctly resolved, corresponding to shallow, moderately conductive weathered materials that provide effective near-surface attenuation. At the same time, several areas that are classified as moderately protected by conductance are downgraded in the DWGVI representation, especially around VES 10–12 and the southern section of the area, where lower.

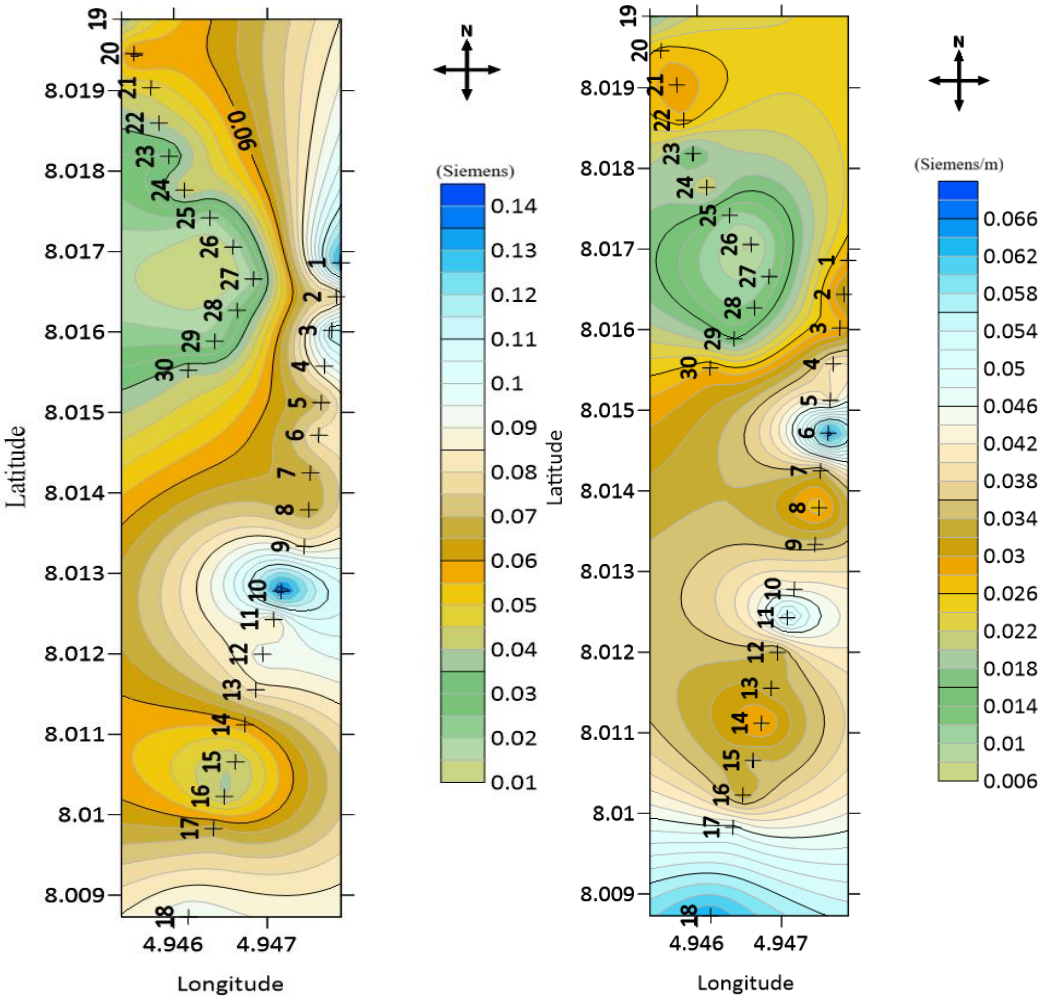

Figure 4: (a) Spatial Distribution Map of Longitudinal Conductance of the Study Area (b) Spatial Distribution Map of DWGVI of the Study Area

Depth-weighted values reflect shallow aquifer conditions and limited overburden effectiveness.

The normalized DWGVI map (Figure 5) reveals pronounced spatial variability in intrinsic groundwater vulnerability across the study area. The distribution highlights distinct vulnerability zones ranging from very low to very high protective capacity, reflecting variations in overburden thickness, lithological composition and aquifer depth. The north-central part of the study area, particularly around VES 24–29, is characterised by very low DWGVIn values, indicated in blue. These zones indicate high intrinsic vulnerability, characterized by shallow aquifer conditions and relatively thin or less conductive protective layers, which reduce the attenuation capacity of the overburden and increase susceptibility of surface-derived contaminants. Localized zones of high DWGVIn are observed around VES 6–7 and in the southern region of the map, indicating areas of relatively low vulnerability and stronger aquifer protection. These zones are associated with thicker weathered materials and moderately conductive shallow layers that enhance contaminant attenuation. The central part of the study area exhibits predominantly moderate $DWGVI_n$ values, suggesting intermediate protective conditions where the balance between overburden thickness and aquifer depth results in moderate intrinsic vulnerability.

The predominance of weak to moderate protective conditions observed in the present study is consistent with previous investigations conducted within the Precambrian basement complex of southwestern Nigeria, where thin overburden development and fracture-controlled occurrence have been associated with intrinsic vulnerability (Bayewu et al., 2018). Similar observations have been reported in other basement terrains,

highlighting the challenges of groundwater protection in environments characterized by discontinuous weathered horizons and heterogeneous fracture networks (Akintorinwa et al., 2020).

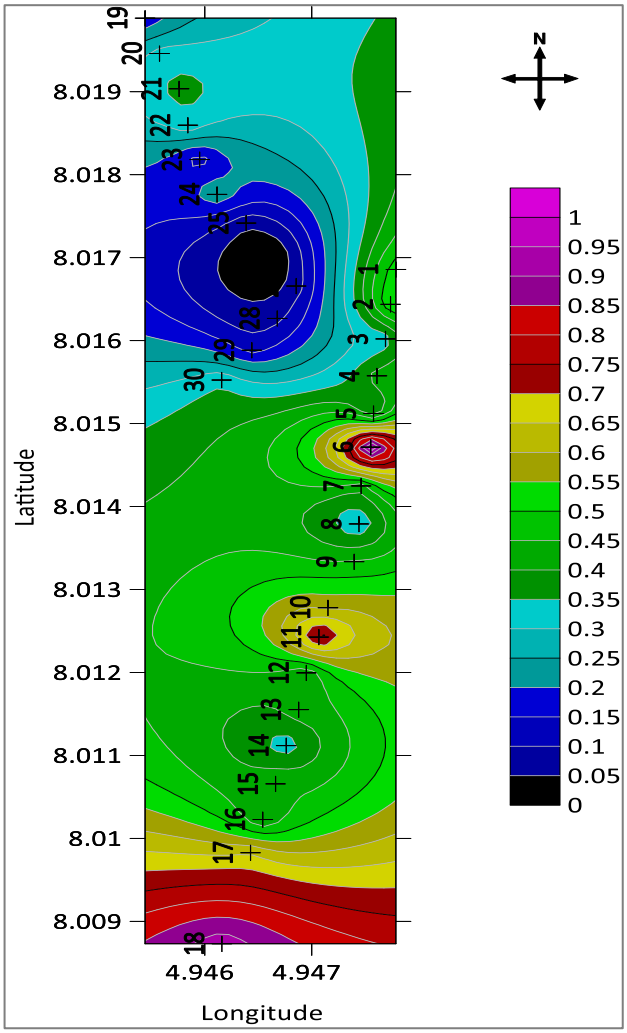

Figure 5: Spatial Distribution Map of $DWGVI_n$ of the Study Area

CONCLUSION

This study proposed and preliminarily evaluated a depth-weighted geoelectrical vulnerability index (DWGVI) for the assessment of intrinsic groundwater vulnerability. The DWGVI explicitly accounts for the vertical distribution of protective layers, addressing limitations inherent to conventional longitudinal conductance methods. Results show substantial spatial variability in aquifer protective capacity, with high DWGVI values corresponding to zones of thick, shallow, conductive weathered layers and low values indicating thin overburden or shallow fractured basement. Longitudinal conductance values ranged from 0.0155 to 0.1439 S, whereas DWGVI values ranged between 0.00744 and 0.06829 S/m. A moderate positive Pearson correlation ($r = 0.607$, $p = 0.00038$) and a stronger Spearman rank correlation ($\rho = 0.740$, $p = 0.001$) indicate that, while general trends are similar, the DWGVI provides an alternative representation of intrinsic vulnerability by incorporating the vertical position of protective layers.

The observed differences between the indices indicate that depth-sensitive weighting may provide an alternative perspective on intrinsic groundwater vulnerability in a basement aquifer environment. The identified vulnerability zones are interpreted as relative indicators of susceptibility rather than direct evidence of existing groundwater contamination. Also, the proposed DWGVI remains preliminary work that has not yet been independently validated. Further studies integrating hydrochemical analyses, microbial indicators, groundwater levels and contaminant-source inventories are required to assess the predictive validity of the proposed index. Furthermore, the study's findings are based on a single institutional case study area underlain by crystalline basement rocks. Consequently, caution should be taken in generalizing the observed vulnerability patterns of the DWGVI to other hydrological settings without further evaluation.

SUPPLEMENTARY MATERIAL

Available with the online version

REFERENCES

Abd-Elaty, I., Kuriqi, A., Ahmed, A., & Ramadan, E. M. (2024). Enhanced groundwater availability through rainwater harvesting and managed aquifer recharge in arid regions. Applied Water Science, 14(6), 121. [Crossref]

Adamu, M. A., Liman, N. C., Usman, N., Muhammad, S. B., & Abdulkadir, A. (2025). Investigation of Groundwater Potential at Fatima Shema Housing Estate Katsina Northern Nigeria. UMYU Scientifica, 4(2), 67–75. [Crossref]

Adebisi, W. A., Afolabi, F., & Babalola, K. K. (2026). Integrated magnetic and electrical sounding investigation of groundwater potential zones in Federal University of Health Sciences, Ila-Orangun permanent site. Discover Geoscience, 4(1), 18. [Crossref]

Akanbi, O. A. (2018). Hydrogeological characterization and prospect of basement Aquifers of Ibarapa region, southwestern Nigeria. Applied Water Science, 8(3), 89. [Crossref]

Akintorinwa, O. J., Atitebi, M. O., & Akinlalu, A. A. (2020). Hydrogeophysical and aquifer vulnerability zonation of a typical basement complex terrain: A case study of Odode Idanre southwestern Nigeria. Heliyon, 6(8), e04549. [Crossref]

Akinwumiju, A. S., & Olorunfemi, M. O. (2018). A GIS-based aquifer vulnerability assessment in the basement complex terrain of southwestern Nigeria. Sustainable Water Resources Management, 4(4), 715–734. [Crossref]

Alao, J. O., Bello, A., Lawal, H., & Abdullahi, D. (2024). Assessment of groundwater challenge and the sustainable management strategies. Results in Earth Sciences, 2, 100049. [Crossref]

Alao, J. O., Yusuf, M. A., Nur, M. S., Nuruddeen, A. M., Ahmad, M. S., & Jaiyeoba, E. (2023). Delineation of aquifer promising zones and protective

capacity for regional groundwater development and sustainability. SN Applied Sciences, 5(5), 149. [Crossref]

Barbulescu, A. (2020a). Assessing Groundwater Vulnerability: DRASTIC and DRASTIC-Like Methods: A Review. Water, 12(5), 1356. [Crossref]

Barbulescu, A. (2020b). Assessing Groundwater Vulnerability: DRASTIC and DRASTIC-Like Methods: A Review. Water, 12(5), 1356. [Crossref]

Barranco, F. T., Saalfield, S. L., Tenbus, F. J., & Shedd, B. P. (2012). Subsurface fate and transport of chemicals. In J. S. Gulliver (Ed.), Transport and Fate of Chemicals in the Environment (pp. 335–368). Springer New York. [Crossref]

Bayewu, O. O., Oloruntola, M. O., Mosuro, G. O., Laniyan, T. A., Ariyo, S. O., & Fatoba, J. O. (2018a). Assessment of groundwater prospect and aquifer protective capacity using resistivity method in Olabisi Onabanjo University campus, Ago-Iwoye, Southwestern Nigeria. NRIAG Journal of Astronomy and Geophysics, 7(2), 347–360. [Crossref]

Bayewu, O. O., Oloruntola, M. O., Mosuro, G. O., Laniyan, T. A., Ariyo, S. O., & Fatoba, J. O. (2018b). Assessment of groundwater prospect and aquifer protective capacity using resistivity method in Olabisi Onabanjo University campus, Ago-Iwoye, Southwestern Nigeria. NRIAG Journal of Astronomy and Geophysics, 7(2), 347–360. [Crossref]

De Almeida, A., Maciel, D. F., Sousa, K. F., Nascimento, C. T. C., & Koide, S. (2021). Vertical electrical sounding (VES) for estimation of hydraulic parameters in the porous aquifer. Water, 13(2), 170. [Crossref]

Egbueri, J. C., Agbasi, J. C., Onuba, L. N., Nweke, N. D., Uwajingba, H. C., & Abba, S. I. (2025). Groundwater development within the Nigerian crystalline and sedimentary aquifers: Challenges and opportunities. In S. Ali & A. Negm (Eds.), Groundwater in Developing Countries (pp. 297–325). Springer Nature Switzerland. [Crossref]

Fannakh, A., & Farsang, A. (2022). DRASTIC, GOD, and SI approaches for assessing groundwater vulnerability to pollution: A review. Environmental Sciences Europe, 34(1), 77. [Crossref]

Hassan, M., & Rilwanu, T. Y. (2025). Characterization and Delineation of Aquifer Potential Zones in Basement Terrain in Parts of Mani Town, Katsina State, Nigeria. *UMYU Scientifica*, *4*(1), 128-136. [Crossref]

Idowu, I. O., & Ojo, A. O. (2024). Exploring groundwater resources in southwestern Nigeria: An integrated geophysical approach. HydroResearch, 7, 213–224. [Crossref]

Ikpe, E. O., Ekanem, A. M., George, N. J., & Thomas, J. E. (2025). Geophysical assessment of aquifer protectivity, groundwater potential and flow dynamics in Northern Akwa Ibom state, Nigeria: Implications for sustainable freshwater management. Geosystems and Geoenvironment, 4(3), 100401. [Crossref]

Jain, H. (2023). Groundwater vulnerability and risk mitigation: A comprehensive review of the techniques and applications. Groundwater for Sustainable Development, 22, 100968. [Crossref]

Karandish, F., Liu, S., & De Graaf, I. (2025). Global groundwater sustainability: A critical review of strategies and future pathways. Journal of Hydrology, 657, 133060. [Crossref]

Lawal, A. A., & Usman, N. (2022). Application of Vertical Electrical Sounding for the Investigation of groundwater potentials at Umaru Musa Yar'adua University, Katsina. UMYU Scientifica, 1(1), 292–302. [Crossref]

Li, P., & Elumalai, V. (2025). Hydrogeology and the global significance of groundwater. In P. Li, X. He, J. Wu, & V. Elumalai (Eds.), Sustainable Groundwater and Environment: Challenges and Solutions (pp. 1–20). Springer Nature Switzerland. [Crossref]

Maria, R. (2018). Comparative studies of groundwater vulnerability assessment. IOP Conference Series: Earth and Environmental Science, 118, 012018. [Crossref]

Nyika, J., & Dinka, M. O. (2023). Introduction to water resources of sub-Saharan Africa. In J. Nyika & M. O. Dinka, Water Challenges in Rural and Urban Sub-Saharan Africa and their Management (pp. 1–15). Springer Nature Switzerland. [Crossref]

Obaje, N. G. (2009). The basement complex. In N. G. Obaje, Geology and Mineral Resources of Nigeria (Vol. 120, pp. 13–30). Springer Berlin Heidelberg. [Crossref]

Ohenhen, L. O., Mayle, M., Kolawole, F., Ismail, A., & Atekwana, E. A. (2023). Exploring for groundwater in sub-Saharan Africa: Insights from integrated geophysical characterization of a weathered basement aquifer system, central Malawi. Journal of Hydrology: Regional Studies, 47, 101433. [Crossref]

Omo-Okoro, P., Ofori, P., Amalapridman, V., Dadrasnia, A., Abbey, Lord, & Emenike, C. (2025). Soil pollution and its interrelation with interfacial chemistry. Molecules, 30(12), 2636. [Crossref]

Oyeyemi, K. D., Aizebeokhai, A. P., Metwaly, M., Omobulejo, O., Sanuade, O. A., & Okon, E. E. (2022). Assessing the suitable electrical resistivity arrays for characterization of basement aquifers using numerical modeling. Heliyon, 8(5), e09427. [Crossref]

Patel, P., Mehta, D., & Sharma, N. (2022). A review on the application of the DRASTIC method in the assessment of groundwater vulnerability. Water Supply, 22(5), 5190–5205. [Crossref]

Sani, Y., Usman, N., Bagudo, I. M., & Albaba, A. L. (2025). Integrated 1-D Resistivity and GIS Analysis for Groundwater Potential Mapping at Umaru Musa Yar'adua University, Katsina

(Nigeria). UMYU Scientifica, 4(3), 296–305. [Crossref]

Sharp, J. M. (Ed.). (2014). Fractured Rock Hydrogeology (0 ed.). CRC Press. [Crossref]

Shuaibu, A. M. (2024). Application of Combined Geoelectrical Techniques for Groundwater Exploration at Federal University Gusau, Zamfara and its Environ, Northwest Nigeria. UMYU Scientifica, 3(4), 244–159. [Crossref]

Tijani, M. N., Obini, N., & Inim, I. J. (2021). Estimation of aquifer hydraulic parameters and protective capacity in basement aquifer of south-western Nigeria using geophysical techniques. Environmental Earth Sciences, 80(14), 466. [Crossref]

Udosen, N. I., Ekanem, A. M., & George, N. J. (2024). Geo-electrical prognosis of aquifer protectivity, corrosivity, and vulnerability via index-based models within a major coastal milieu. Discover Geoscience, 2(1), 18. [Crossref]

You, X., Liu, S., Dai, C., Guo, Y., Zhong, G., & Duan, Y. (2020). Contaminant occurrence and migration between high- and low-permeability zones in groundwater systems: A review. Science of The Total Environment, 743, 140703. [Crossref]